

Influence of flexural loading on chloride ingress in concrete subjected to cyclic drying-wetting condition

Hailong Ye^{1,3a}, Chuanqing Fu^{1,2}, Nanguo Jin^{*1b} and Xianyu Jin¹

¹Department of Civil Engineering, Zhejiang University, 388 Yuhangtang Road, Hangzhou 310058, China

²College of Civil Engineering and Architecture, Zhejiang University of Technology, Hangzhou, 310014, China

³Department of Civil and Environmental Engineering, The Pennsylvania State University, 3127 Research Drive, State College, PA, 16801, USA

(Received April 30, 2012, Revised November 16, 2014, Accepted December 16, 2014)

Abstract. Chloride ingress implies a complex interaction between physical and chemical process, in which heat, moisture and chloride ions transport through concrete cover. Meanwhile, reinforced concrete structure itself undergoes evolution due to variation in temperature, relative humidity and creep effects, which can potentially change the deformation and trigger some micro-cracks in concrete. In addition, all of these process show time-dependent performance with complex interaction between structures and environments. In the present work, a time-dependent behavior of chloride transport in reinforced concrete beam subjected to flexural load is proposed based on the well-known section fiber model. The strain state varies because of stress redistribution caused by the interaction between environment and structure, mainly dominated by thermal stresses and shrinkage stress and creep. Finally, in order to clear the influence of strain state on the chloride diffusivity, experiment test were carried out and a power function used to describe this influence is proposed.

Keywords: concrete structure; chloride ingress; section fiber model; strain state; external loadings

1. Introduction

Chloride-induced corrosion of steel reinforcement is a major cause affecting the service life of reinforced concrete (RC) structure exposed to marine environments. Chloride-induced corrosion begins when the chloride concentration at the steel bars reaches a threshold value, which can destroy the protective layer formed around rebars by changing the initial high pH environments. The corrosion of steel can reduce the cross section area of rebar and diminish its bonding capability with concrete, which can further degrade the structural loading capability and sustainability. Therefore, an accurate prediction of the initiation corrosion time in RC structures is necessarily crucial in term of durability design and service-life prediction (Van Mien, Stitmannathum *et al.* 2009, Papadakis 2013). However, chloride ingress process implies a complex interaction between physical and chemical process, in which heat, moisture and chloride

*Corresponding author, Professor, Email address: jinng@zju.edu.cn

^aPh.D. Candidate, E-mail address: yehailong1@gmail.com ; huy131@psu.edu

^bPh.D., Professor

ions transport through concrete cover (Bastidas-Arteaga, Chateauneuf *et al.* 2010, Ye, Tian *et al.* 2013, Lin and Yang 2014).

In the previous studies regarding predicting chloride ingress in saturated concrete, environmental conditions (e.g. chloride concentration at surface, ambient temperature) and material properties (e.g. chloride diffusivity) were generally treated as a series of constants or simple time functions, with no considering the loading effects, especially time-dependent forces or dynamic impacts. An example of this simplified case is the proposed Fick's second law, which has been widely implemented by researchers to compute the service life due to its simple mathematic expression (Chatterji 1995). However, most RC structures perform under external loadings coupled with complex interactions with environments in realistic circumstances. As a matter of fact, either the existence of external loading or the triggered local stress in concrete due to boundary constraints, can inevitably result in the initiation, growth, and linking of micro-cracks and reshape the present structural cracks. For instance, the bending member in RC structure served under dynamic vehicle loadings can accumulate its deformation and damage due to fatigue. The changes in concrete microstructure or generation of micro-cracks can accelerate the chloride transport process (Chen and Mahadevan 2008, Yang and Weng 2013, Zhang, Dong *et al.* 2013, Lin and Yang 2014). In particular, under cyclic drying-wetting conditions, the influence of micro-cracks can enhance the complexity of chloride ingress process in concrete. For instance, the crack characteristics (e.g. crack connectivity, crack width) can potentially play as the capillaries for capillary action, which can accelerate the water suction and chloride ingress.

As a survey of previous investigation, the coupling interactions between external loadings and environments are rarely elucidated or considered, despite various models in predicting initial corrosion time has been proposed. For example, Bastidas-Arteaga *et al.* presented a stochastic approach to assess chloride ingress into concrete considering the effects of chloride binding, temperature, humidity, concrete aging and convection by combining the finite element formulation with finite difference. However, they did not consider the kinematics between concrete cracking, microstructure evolution. and chloride penetration (Bastidas-Arteaga, Chateauneuf *et al.* 2010); Cheung *et al.* provided an approach to simulate the corrosion initiation process under dynamic environmental conditions, and demonstrated that the annual variation of the environmental conditions, such as temperature, humidity, and surface chloride concentration, have a very significant impact on the corrosion initiation process in RC bridges. But the reaction of structures and in turn influence on environment were not contained in this particular case (Van Mien, Stitmannathum *et al.* 2011, Cheung, So *et al.* 2012, Paul, Chaudhuri *et al.* 2014).

One the other hand, the existence of external loadings can potentially generate cracks in concrete. Admittedly, large surface cracks are undesirable since wide cracks can probably permit greater migration of moisture, chloride ions, and oxygen through concrete cover. In addition, the alteration of loading status can potentially change cracking state, for instance, unloading probably induces partially crack closure. Furthermore, the evolving strain or stress states can affect the chloride ion transport process in concrete depending on the history and present loading and environmental status. Recently, the relationship between the sustained strain or stress state with chloride diffusivity were investigated by many researchers. For example, Saito and Ishimori found that the chloride permeability increase with the increase of residual strains and only the residual strains can potentially contribute to chloride transport (Saito and Ishimori 1995). Lim *et al.* studied the chloride diffusivity under sustained compressive and tensile loads and found that the coefficient in tensile zone was relatively higher than that of compressive zone (Lim, Gowripalan *et al.* 2000). Van Mien, T presented a model to predict the chloride diffusion coefficient in tensile

zone of plain concrete under flexural cyclic load and found that the chloride diffusion increases with increasing load levels (Van Mien, Stitmannathum *et al.* 2011). They also investigated the effects of cyclic flexural loads on chloride diffusion characteristics of plain concretes, and proposed a model to predict the chloride penetration into plain concretes subjected to both tidal environments and different cyclic flexural load levels (Van Tran, Stitmannathum *et al.* 2009). However, it is hard for researchers to reach an agreement on this issue so far.

In this study, a numerical model considering the coupling effects between dynamic environments and structure is established and applied to reinforced concrete beam members subjected to chloride environments and flexural forces. The time-dependent behaviors of structure are mainly based on the simulation of crack propagation caused by heat, moisture, (i.e. thermal cracking and drying shrinkage cracking) and material creep based on CEB-FIP, as well as the widely-known section fiber model. In particular, in order to make clear the influence of strain state on the change of chloride diffusivity, experiment test were carried out and a power function used to describe the influence is proposed in present work.

2. Governing equations

2.1 Heat transport

Fourier's heat conduction law is used as governing equation of heat transport in RC concrete for temperature prediction (Bažant and Najjar 1972, Ababneh, Benboudjema *et al.* 2003):

$$\rho_c c_p \frac{\partial T}{\partial t} = \text{div}(k_c \nabla T) \quad (1)$$

where T is concrete temperature; ρ_c is concrete density; c_p is specific heat of concrete; k_c is thermal conductivities of concrete, based on the research of Jeong *et al.*, the thermal conductivity can be expressed a function of the temperature T in addition to moisture humidity h and degree of hydration α (Jeong and Zollinger 2006):

$$k_c = a \ln \left[\frac{1}{\alpha} \left(-\ln \frac{1}{T} \right)^h \right] + b \quad (2)$$

where a and b are laboratory-derived coefficients.

2.2. Moisture diffusion

The conservation of mass equation for moisture transport in concrete can be expressed as (Bažant and Najjar 1972, Ababneh, Benboudjema *et al.* 2003):

$$\frac{\partial w_e}{\partial t} = \frac{\partial w_e}{\partial h} \frac{\partial h}{\partial t} = \text{div}(D_h \nabla(h)) \quad (3)$$

where w_e is total water content; h is pore relative humidity; $\partial w_e / \partial h$ is moisture capacity, which

depend on the properties of material; D_h is permeability which can be obtained from a reference value $D_{h,ref}$ by timing correction factor, considering temperature $f_{h,2}(T)$, humidity $f_{h,3}(h)$ and age $f_{h,1}(t)$, respectively (Bažant and Najjar 1972, Ababneh, Benboudjema *et al.* 2003):

$$D_h = D_{h,ref} (w/c) \cdot f_{h,1}(t) \cdot f_{h,2}(T) \cdot f_{h,3}(h) \quad (4)$$

where, especially, the reference value of diffusivity can be expressed as a function of water-cement (w/c) ratio of concrete proposed by many researchers (Fu, Jin *et al.* 2010).

2.3 Chloride ions Ingress

The diffusion model of chloride ions permeate in unsaturated concrete can be expressed as (Bažant and Najjar 1972, Ababneh, Benboudjema *et al.* 2003):

$$\frac{\partial C_f}{\partial t} = \frac{\partial C_f}{\partial C_t} \left(\text{div} [D_{cl} \nabla (C_f)] + \mu \frac{\partial w}{\partial t} C_f \right) \quad (5)$$

where C_t is total concentration of ions in grams of total chloride per gram of concrete; C_f is free concentration of ions in grams of free chloride per gram of concrete; D_{cl} is chloride diffusivity of concrete; $\partial C_f / \partial C_t$ is binding capacity of concrete; μ is unit converter to grams of chloride per gram of concrete. The chloride diffusivity can also be determined also by timing correction factor considering the influence of temperature $f_{cl,2}(T)$, humidity $f_{cl,3}(h)$, age $f_{cl,1}(t)$ and free chloride concentration $f_{cl,4}(C_f)$ (Bažant and Najjar 1972, Ababneh, Benboudjema *et al.* 2003):

$$D_{cl} = D_{cl,ref} (w/c) \cdot f_{cl,1}(t) \cdot f_{cl,2}(T) \cdot f_{cl,3}(h) \cdot f_{cl,4}(C_f) \quad (6)$$

The reference value of diffusivity of chloride is also based on the water-cement ratio. The binding capacity $\partial C_f / \partial C_t$ varies from different type and can be determined experimentally. The detail of each can be found according to the research of Bažant and Najjar *et al.*

3. Time-dependent deterioration model

Time-dependent development in material properties of concrete (i.e. strength and modulus of concrete, creep coefficient) is based on the CEB-FIP model, which takes account of numerous parameters, such as cement type, ambient temperature, relative humidity, concrete strength and concrete age.

3.1 Time-dependent thermal strain

The relationship between temperature variation and the associated time-dependent thermal strain at any point of the cross-section of structural members can be expressed as (Chen and

Mahadevan 2008):

$$\varepsilon_T(t) = \alpha_T \cdot [T(t) - T_0] \quad (7)$$

where $\varepsilon_T(t)$ is thermal strain; α_T is thermal expansion coefficient depending on temperature and moisture content. However, in the present work, in order to emphasize the influence of structural loading on the chloride penetration, the experiments presented below are tested at constant environment temperature, indicating this influence is ignored in this particular case.

3.2 Time-dependent shrinkage strain

The relationship between moisture content variation and the associated time-dependent mechanical strain (i.e., wetting expansion/drying shrinkage strain) can be expressed as (Code 1993):

$$\varepsilon_{sh}(t) = \varepsilon_{sh0} \beta_H \left[\frac{(t-t_0)}{350(2A_c/100u)^2 + (t-t_0)} \right]^{0.5} \quad (8)$$

where, ε_{sh} is shrinkage strain; ε_{sh0} is the notional shrinkage and A_c is the cross-sectional area and u is the perimeter in contact with the atmosphere; β_H is a function of the relative humidity:

$$\beta_H = \left\{ \begin{array}{l} -1.55 \left[1 - \left(\frac{h}{100} \right)^3 \right] \quad 40\% \leq h \leq 99\% \\ +0.25 \quad h \geq 99\% \end{array} \right\} \quad (9)$$

3.3 Time-dependent strain due to creep

In addition, concrete material can creep under external loadings, which enlarges the structural deformation and induce microstructure evolution. If creep were free to occur, the time-dependent creep strain $\varepsilon_{creep}(t)$ would increase during the period by the amounts (MacGregor 1988):

$$\varepsilon_{creep}(t) = \phi(t) \varepsilon(t_0) \quad (10)$$

where $\varepsilon(t_0)$ is initial stress; $\phi(t)$ is creep coefficient, which can be determined using the CEB-FIP model from the following hyperbolic power function (Code 1993):

$$\phi(t) = \left[1 + \frac{1-h/h_0}{0.46(2A_c/100u)^{1/3}} \right] \left(\frac{5.3}{\sqrt{0.1f_{cm28}}} \right) \left(\frac{1}{0.1+t_0^{1/5}} \right) \times \left[\frac{t-t_0}{\beta_H + (t-t_0)} \right]^{0.3} \quad (11)$$

where h is relative environmental humidity; h_0 equals to 100%; f_{cm28} stands for the mean compressive strength at the age of 28 days, and

$$\beta_H = \min \left\{ 1, 500; 150 \left[1 + (1.2h)^{18} \right] \frac{2A_c}{100u} + 250 \right\} \quad (12)$$

where the parameters are same are same with Eq. (8).

3.4 Time-dependent analysis of beam based on fiber section model

Assuming a RC beam member subjected to flexural loads, the sections can be divided into two forms according to cracking or not cracking along the span. In the present work, it is assumed that during the time-dependent analysis, the cracks caused by temperature, shrinkage and creep effects merely contribute the stress redistribution but not onset the new cracks besides structural cracks. In addition, the stress redistribution of cracked or un-cracked sections may influence the strain state of section of any fiber, which in turn affects the chloride ingress.

Consider a RC beam due to the application of a positive bending moment M and force N at an arbitrarily chosen point O . The instantaneous strain and stress distribution immediately after application of force is assumed to be available at initial age t_0 . Whether the section is cracked or not, the total change in strain of any fiber $\Delta\varepsilon_i(t)$ at time t_0 due to creep, shrinkage and temperature occurring between t_0 and t can be expressed as (MacGregor 1988):

$$\Delta\varepsilon_i(t) = \varepsilon_{creep,i}(t) + \varepsilon_{sh,i}(t) + \varepsilon_{T,i}(t) \quad (13)$$

where $\varepsilon_{creep,i}(t)$, $\varepsilon_{sh,i}(t)$ and $\varepsilon_{T,i}(t)$ represent the changes of strains at fiber i due to creep shrinkage and temperature. For cracked section, the fibers in tension is free of stress and total change equals zero, not including the fiber representing steel and other material in high tension stress capacity. Based on the fiber section model, the strain distribution is assumed to be linear across the section, at any fiber i , at a distance y from the reference point O , the strain always can be expressed as a function of the strain at the reference point and curvature by integrating of the total change in stress over the area of the cross-section. The equivalent force produced by creep, shrinkage and temperature can be expressed as:

$$\begin{Bmatrix} \Delta N(t) \\ \Delta M(t) \end{Bmatrix} = \begin{Bmatrix} \int_{A_c} \Delta\sigma_y(t) dA \\ \int_{A_c} \Delta\sigma_y(t) \cdot y dA \end{Bmatrix} = \int \mathbf{B}_s^T E_c(t) \mathbf{B}_s \begin{Bmatrix} \Delta\varepsilon_o(t) \\ \Delta\psi(t) \end{Bmatrix} = \mathbf{K}_s(t, t_0) \begin{Bmatrix} \Delta\varepsilon_o(t) \\ \Delta\psi(t) \end{Bmatrix} \quad (14)$$

where $\mathbf{B}_s = [1 \ y]$, $\mathbf{K}_s(t)$ is section stiffness matrix $E_c(t, t_0)$ is tangent modulus. In un-cracked section, strain changes due to creep, shrinkage and temperature result in time-dependent stress redistribution among the various materials. While, in a fully cracked section, only the area subjected to compression is considered effective in resisting the internal forces. Creep, shrinkage and temperature generally result in a shift of the neutral axis towards the bottom of the section. To avoid this difficulty, the effective area of the cracked section is assumed to be unchanged and the increased part in compression is neglected. The resulting axial strain and curvature are obtained by:

$$\begin{Bmatrix} \Delta \varepsilon_o(t) \\ \Delta \psi(t) \end{Bmatrix} = \mathbf{K}_s^{-1}(t, t_0) \begin{Bmatrix} \Delta N(t) \\ \Delta M(t) \end{Bmatrix} \quad (15)$$

Eq. (15) gives a relationship between the force and strain for any cross sections. There is one point should be emphasized, in a fully cracked section the section stiffness matrix $\mathbf{K}_s(t)$ should contain the fiber of equivalent area standing for steel in the tension areas, while differently, the increased axial force and bending moment caused by creep, shrinkage and temperature only consider the fiber in the compression areas.

3.5 Stress-strain relationship

The monotonic stress-strain relationship served as a reasonable envelope for the peak values of stress for concrete during the service life when the hysteretic loop intersects with the descending branch of the envelope cures. In the present work, the Saenz formula is adopted to describe the stress-strain cure under uniaxial compression, it can be expressed as (Chen 2007):

$$\sigma = \frac{E_0 \varepsilon}{1 + (E_0/E_s - 2)(\varepsilon/\varepsilon_0) + (\varepsilon/\varepsilon_0)^2} \quad (16)$$

where, ε_0 is the peak strain; E_0 is the initial tangential modulus, E_s is the secant modulus taken at the compressive strength f_c . In present research, tangent modulus is adopted more important, thus, Eq. (35) can be rewritten as the form of increment, which resulting the tangential modulus:

$$E_{c,i} = \frac{d\sigma_i}{d\varepsilon_i} = \frac{[1 - (\varepsilon_i/\varepsilon_0)^2] E_0}{[1 + (E_0/E_s - 2)(\varepsilon_i/\varepsilon_0) + (\varepsilon_i/\varepsilon_0)^2]^2} \quad (17)$$

It can be seen that the tangent modulus is different for each fiber along the cross-section in favor of the different strains. For uniaxial tension, the concrete is assumed as a quasi-brittle material. The stress-strain relationship can be expressed as following, where, it was separated into ascending branch and descending branch, which bridges a relationship with the crack width (Chen 2007):

$$\sigma = \begin{cases} f_t \left[1 - (1 - \varepsilon/\varepsilon_{t,p})^\alpha \right] & \text{ascending branch} \\ f_t e^{-k w \lambda} & \text{descending branch} \end{cases} \quad (18)$$

where $\alpha = E_t \varepsilon_{t,p} / f_t$; w is the crack width; E_t is initial tangent modulus; λ and k are parameters.

4. Solution procedure

Fig. 1 depicts the algorithm used to determine the time-dependent variation of the profiles of

1. Determining whether element has cracked or not based on the initial material property and external force. The element is assumed to be cracked when the tensile stress reaches the critical cracking strength. After that, a re-distribution of stress is analyzed to that particular section.
2. According to the initial and boundary conditions, determining the temperature, humidity profile for the un-cracked sections based on Eqs. (1) and (3). In the case of cracked section, the temperature and relative humidity in cracked region can be approximated to be identical to environments. Whilst for the un-cracked regions in the cracked element, the determination is similar to un-cracked section.
3. Determining the change of strain of each fiber for each section due to creep, temperature and shrinkage based on the initial stress, material properties, temperature and humidity profiles.
4. Calculating the change of strain and stress based on the fiber section model and material constitutive law. Noting that in this step, some un-cracked section may change into crack section due to the environment factors, and have to be re-calculated. The final changes in strain and stress will influence the transport of humidity and chloride in the following time.
5. Determining the chloride profile in the cracked and un-cracked element.

5. Experimental procedure

As introduced before, the beam sections can be classified into cracked and un-cracked one according to cracking status. For cracked sections, numerous investigation have been documented regarding the influence of macro-cracks on chloride penetration process subjected to cyclic drying-wetting condition experimental (Ye, Jin *et al.* 2012, Ye, Tian *et al.* 2013). Hence the following experiments focus on the influence of relative small amount of external loading (i.e. less than 30% of ultimate strength) on chloride penetration process. Under that circumstance, macro-cracks are not be able to visible detected and assume that only micro-cracks exist in concrete, which can potentially alter the chloride profiles in concrete.

5.1 Material and mixing proportion

Ordinary portland cement (ASTM Type I 32.5), added by 5% $\text{CaSO}_4 \cdot 2\text{H}_2\text{O}$, was used in all mixtures. Crushed gravel with continuous grading rang from 5 mm to 20 mm was used as the coarse aggregate and maximum aggregates size was 20 mm. Natural sand with good particle grading and fineness modulus of 2.64 was used. Table 1 lists the mix proportions of the concrete used in this study.

5.2 Details of specimens

The specimen configuration is shown in Fig. 2. The specimen had a rectangular cross section of 160 mm \times 100 mm, with a total length of 1400 mm. In addition, 2 Φ 12 HRB 335, 2 Φ 8 HRB335 and Φ 6@100HPB 235 in Chinese Standard was used as tensile and compressive reinforcements and hooping in these specimens. At either end of the specimens, a PVC pipes were reserved for later loading. All specimens were subjected to a initial curing in the environment of 90%RH and $20 \pm 3^\circ\text{C}$ for 28days after removal from the mold since 24 hours. The sustaining loads were applied according to the internal self-balancing methods based on the mechanism of tightening nuts and transporting force to compressive springs, whose values can be measured by slide caliper as a tag

Table 1 Mixing ingredient of concrete (kg/m³).

w/c	Cement	Fine aggregate	Coarse aggregate	Water
0.53	370	750	1112	188

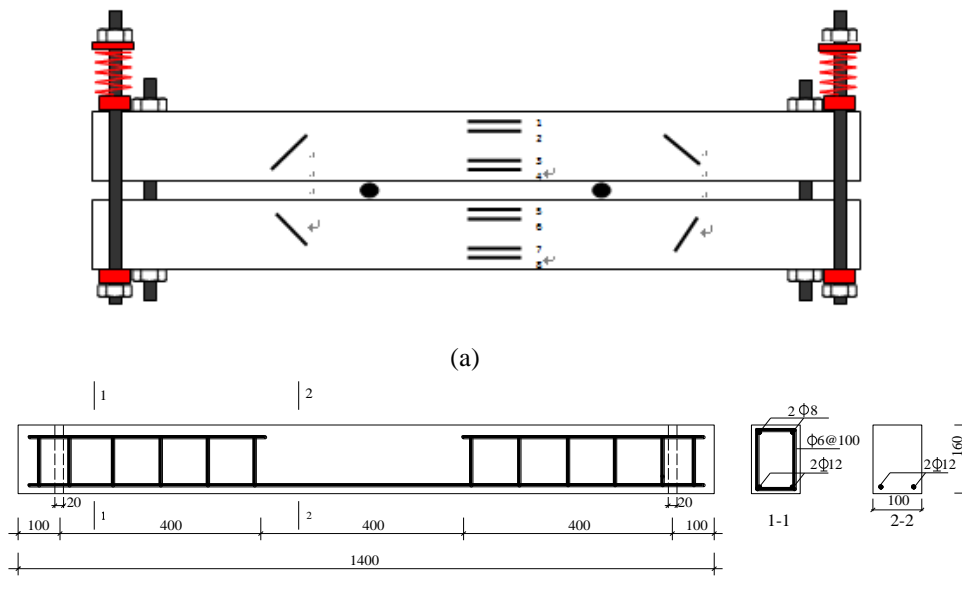


Fig. 2 Configuration of a specimen (a) details of loading systems (b) the details of steel distribution in RC beam



Fig. 3 (a) Loading application and (b) strain measurements Fu, Ye, *et al.* 2015

for the class of loadings. The correlation between the loading application and the compressed spring lengths was approximately established using a linear function. In addition, in order to research the influence of loading on chloride ingress, four different classes of loadings were applied, i.e., 28%, 22%, 16% and 10% of the ultimate flexural strength, respectively. The purpose

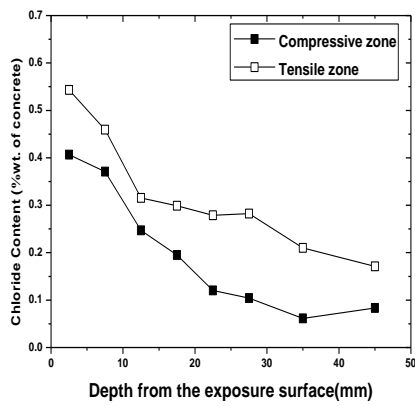
of using relative small loading magnitude is to eliminate the potential visible macro-cracks, and focus on the alteration of microstructure (e.g. elastic deformation of solid skeleton, micro-cracks). Furthermore, strain foils (as labeled in Fig. 2) were also arranged along the section of the cross at the distance from the exposure surface 20 mm (strain foils 1, 8), 40 mm (strain foils 2, 7) for tensile zones and 120 mm (strain foils 3, 6), 140 mm (strain foils 1, 8) for compressive zones to measure the influence of strain of each fiber, as shown in Fig. 3.

The specimens were subjected to accelerated penetration of chloride ions for 90 days through a cyclic drying-wetting test in an automatic test device based on water level sensors and multi-function artificial environment chamber, which can automatically control the environment temperature and humidity. During the test, each cycle of the drying-wetting test consisted in wetting for 18 hours through immersion in a sodium chloride solution (5.0% NaCl) and drying for 6 hours at 60% RH. The environmental temperature is kept constant at 50°C to accelerate the transportation of chloride ions. After the accelerated penetration of chloride ions, concrete samples in both compressive and tensile zones were taken from each specimen to measure the chloride ions content by ZD-2-Automatic Potentiometric Titrator.

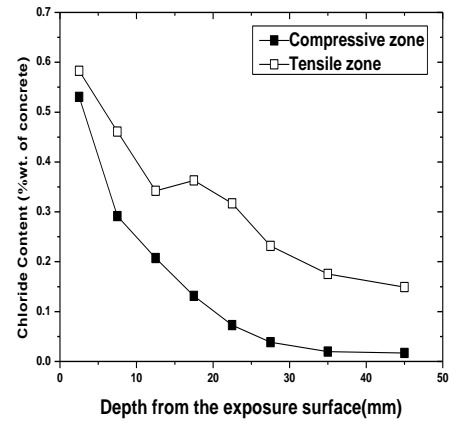
6. Result and discussion

Fig. 4 shows the comparison of chloride ions profiles in tensile zones and compressive zones at different classes of loadings subjected to proposed drying-wetting conditions. It can be seen that for a single certain section subjected to a unique class of loading, the concentration of chloride at the tensile zone is considerably higher than that in compressive zone. This phenomenon can be approximately explained by the intrinsic material property of concrete whose compressive strength is stronger than tensile strength as a quasi-brittle material. But it varies with the strain conditions, when strain is small than a certain value, the difference diminishes which is reflected in the specimens subjected to 10% of the ultimate flexural strength. However, it is hard to determine the value of stress when the influence of stress can be neglected merely based on this test.

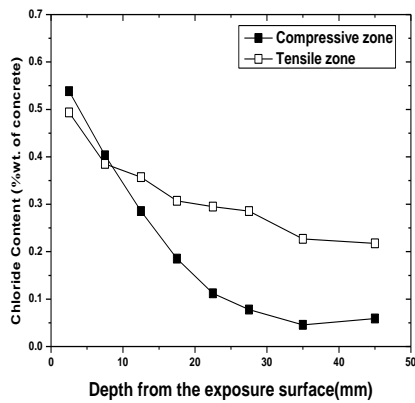
The influence of strains on the chloride profiles both in the tensile zones and compressive zones are shown in Fig. 5. The strains in the compressive zones at the distance of 140 mm are measured to be -186×10^{-6} , -219×10^{-6} , -98×10^{-6} and -91×10^{-6} , while at 120 mm are -71×10^{-6} , -122×10^{-6} , -37×10^{-6} and -49×10^{-6} for 28%, 22%, 16% and 10% of ultimate flexural strength, respectively. However, there are some errors in setting the relationship between the loadings and strains, but it has no influence on establishing the nexus of diffusivity and strains. In the compressive zones, the measured strain has a relationship of $\varepsilon_{22\%} > \varepsilon_{28\%} > \varepsilon_{10\%} > \varepsilon_{16\%}$, indicating that the concentration tends to be larger with the increase of strains. It can be explained by the change in concrete microstructure reflected in porosity and connectivity. With the increase of strain, it can generate inchoate micro-cracks on the weak zone like interfere transition zone (ITZ) region, which somewhat reflects on the enlarger of diffusivity correspondingly; However, it neither demonstrates that the diffusivity simply increases with increase of stress based on the present test, nor any compressive strain can enlarge the diffusivity. Merely for the largest strain in the present test, the chloride profiles locate in the middle disorganize the overall regular pattern. It might be explained that beyond some range of strain, the inchoate micro-cracks can somehow close, with the pore geometry is modified and connectivity is reduced, in turn, counteracting the negative effect and reducing diffusivity.



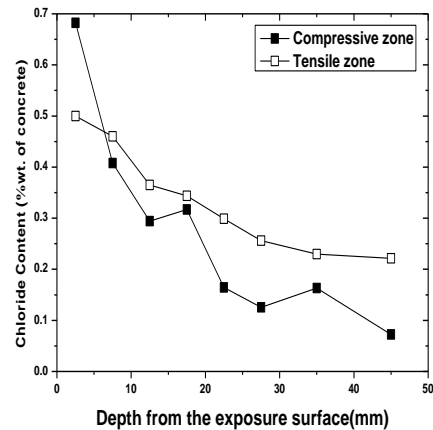
(a)



(b)



(c)



(d)

Fig.4 Comparisons of chloride ions profiles in tensile zone and compressive zone of pure bending section at different classes of loading subjected to the wetting-drying conditions (a)10%; (b)16%; (c) 22%; (d) 28% of ultimate strength

On the other hand, in tensile zones of pure bending section, this trend is not seem be inconspicuous. It is clear that tensile strains stimulate the propagation of micro-cracks in the weak zone, drastically accelerating the diffusivity by breaking a smooth path. The strains in tensile zones at the distance of 20 mm are separately 714×10^{-6} , 321×10^{-6} , 273×10^{-6} and 209×10^{-6} and at the distance of 40 mm are 557×10^{-6} , 256×10^{-6} , 235×10^{-6} and 155×10^{-6} for 28%, 22%, 16% and 10% of ultimate flexural strength, respectively. The strain satisfies a relationship of $\varepsilon_{28\%} > \varepsilon_{22\%} > \varepsilon_{16\%} > \varepsilon_{10\%}$, and it also can be seen that the higher chloride concentration at higher strain is merely obvious at the point about 40 mm depth form exposure surface.

7. Back-calculation of the modified function on chloride diffusivity

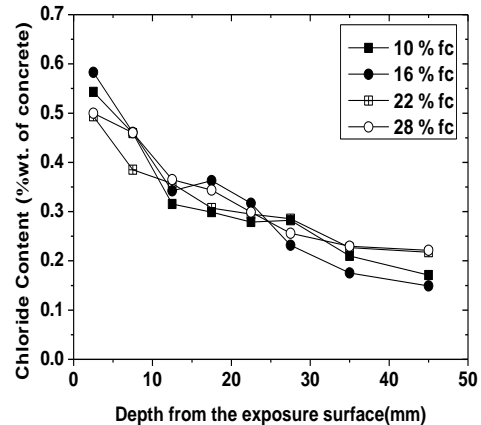
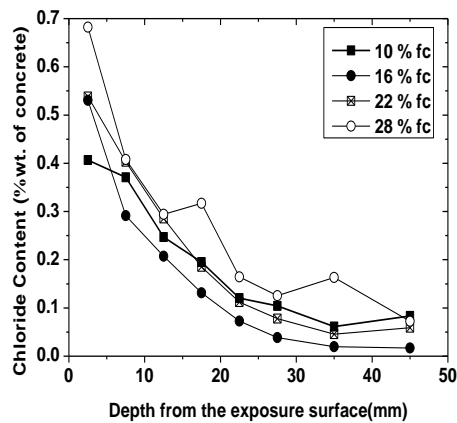
It can be seen that strain state plays an important role on the calculation of diffusivity, and somehow dominates the chloride ions movements in concrete. For better prediction of chloride concentration in a realistic RC structure and for the ease measurement of strain, it is assumed that the influence of strain on the diffusivity can be expressed as a power function of the strain ε and peak strain $\varepsilon_{t(c)p}$ as follows:

$$f_{Cl}(\varepsilon) = a \cdot \left(\frac{\varepsilon}{\varepsilon_{t(c)p}} \right)^b \tag{19}$$

where a and b are the coefficients based on the experimental tests. The application of this regressed equation can be further used to modify the Eq. (6) by considering the strain state of concrete. In order to calculate the coefficients, the strains are assumed to satisfy the plane cross-section assumption, thus based on the experimental results, the strains at any point can be calculated without using the above section fiber model, specially the strains are time-independent.

In addition, for compressive zones, the peak strain are expressed a function of the compressive strength $\varepsilon_{cp} = 0.546 + 0.0291f_{cu}$, while for tensile zone the peak strain also are expressed as a function of the tensile strength $\varepsilon_{tp} = 65 \times 10^{-6} f_t^{0.54}$ (Guo 1997).

In the case of compressive zones, the highest strain level is neglected, by searching for the minimum deviation of the test results and the model, the coefficients a and b equal to 249 and 1.62, respectively. Hence, Eq. (19) can be rewritten as $f_{Cl}(\varepsilon) = 249(\varepsilon/\varepsilon_{cp})^{1.62}$. Based on the above equations, the modified profiles can be drawn as shown in Fig. 6.



(c)

(d)

Fig. 5 (a) Chloride profiles in compressive zone of pure bending section subjected to cyclic wetting-drying conditions; (b) Chloride profiles in tensile zone of pure bending section subjected to cyclic wetting-drying conditions

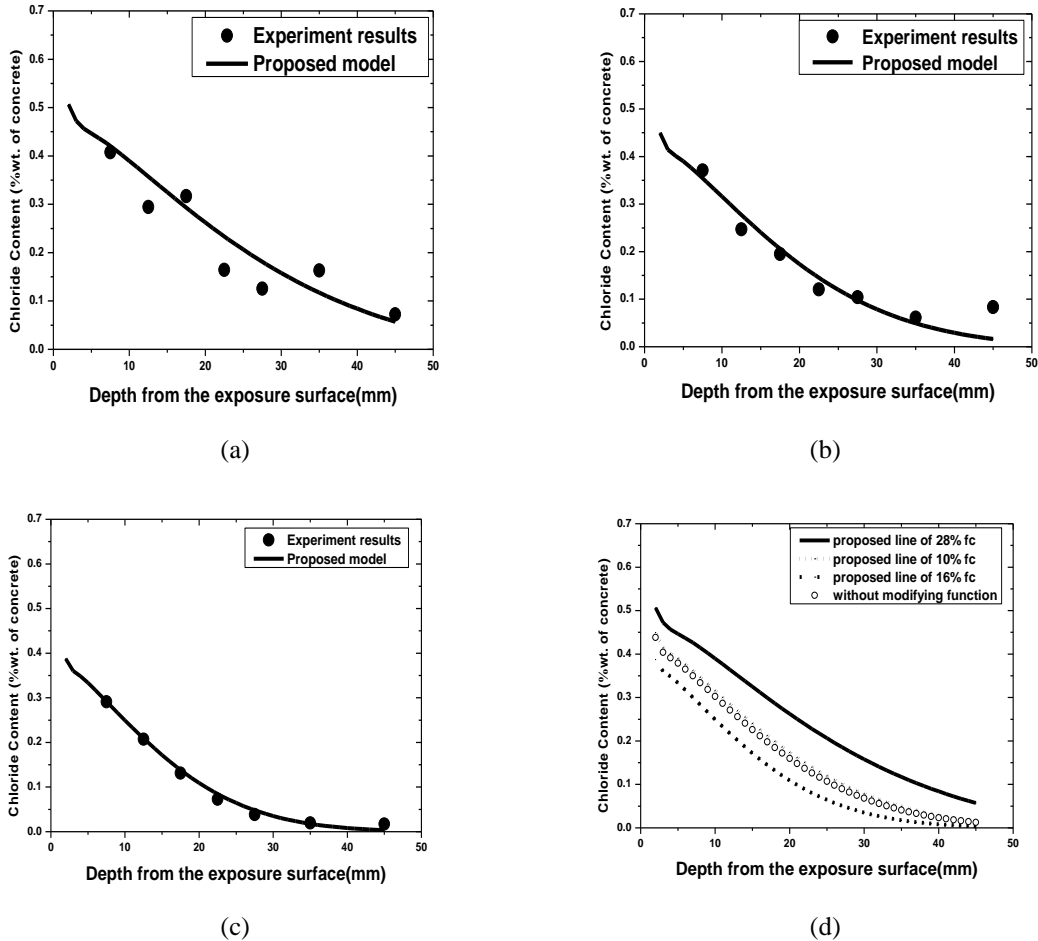


Fig. 6 (a) Comparison of chloride ions profiles of experiment results and proposed line for the loading of 28% ultimate flexural strength; (b) Comparison of chloride ions profiles of experiment results and proposed line for the loading of 10 % ultimate flexural strength; (c) Comparison of chloride ions profiles of experiment results and proposed line for the loading of 16 % ultimate flexural strength; (d) Comparison of chloride ions profiles of proposed line and the line without modifying function

By comparing the chloride profiles of proposed line and line without modifying function (Fig. 6 (d)), it can be seen that at low strain value, approximately lower than 37×10^{-6} , the compressive strain has a positive influence on chloride transport, but while the compressive strain outstrip the critical value, it switches to a negative influence. For tensile zone, because of the inconspicuous difference between experiment results, mainly for the middle period, the aberrant data are neglected and the modifying function is also assumed to have the expression of power function, the coefficients a and b equal 1.77 and 0.67, respectively. Hence, the Eq. 19 can be rewritten as $f_{cl}(\varepsilon) = 1.77(\varepsilon/\varepsilon_p)^{0.67}$. Fig. 7 shows the comparison of chloride profiles of experiment results and proposed line in the tensile zones for the loadings of 28% and 16% ultimate flexural strength.

8. Conclusions

In this paper, the time-dependent behavior of chloride ingress in RC beam subjected to flexural loads is studied. This is the first time to using the section fiber model in dealing with the problem of coupled action of environments and structural loadings for chloride ingress process. Following conclusions can be obtained:

- The time-dependent behavior of RC structure has an important influence on the chloride ingress. By using the well-known section fiber model, the behavior of RC structure bridges a relationship between loading effects with the structural behaviors due to variation in temperature, humidity and creep, which redistributes the stress and strain states.
- Strain state in tension and compression makes a big difference on the chloride profiles in concrete. Tensile strain has a negative influence by straightly accelerating chloride ingress while compressive strains at lower level make positive reducing chloride diffusivity but at high level it makes negative influence as well.
- A formula is established to predict the influence of the strains on the chloride ions transport based on the strains and the peak strain using power functions.
- It is suggested that the strain state of concrete plays an important role on the chloride transport, although the stress level is relative small and may not induce visible macro-cracks. Thus it is necessary to take account of strain state when predicting the initial corrosion time.
- The reliability analysis is not studied here, which is however an important step to estimate the service life in RC structure, since the environments (i.e. weather conditions) and the material properties, are all either random variables or random processes. In addition, the forces applied to RC structure are mostly dynamic and random. Also, the fatigue process, which is also an important factor deteriorating the structure, can induce many micro-cracks and affect chloride ingress. All of these factors are important and should be incorporated in the future investigations.

Acknowledgments

The financial support from the National Basic Research Program (973 Program) (Grant No. 2015CB655100), of the People's Republic of China and the National Natural Science Foundation (Grant Nos. 51478419 and 51320105013) is gratefully acknowledged.

References

- Ababneh, A., Benboudjema, F. and Xi, Y. (2003), "Chloride penetration in nonsaturated concrete", *J. Mater. Civil Eng.*, **15**, 183.
- Bastidas-Arteaga, E., Chateauneuf, A., Sánchez-Silva, M., Bressolette, P. and Schoefs, F. (2010), "A comprehensive probabilistic model of chloride ingress in unsaturated concrete", *Eng. Struct.*, **33**(3), 720-730.
- Bazant, Z. and Najjar, L. (1972), "Nonlinear water diffusion in nonsaturated concrete", *Mater. Struct.*, **5**(1), 3-20.
- Chatterji, S. (1995), "On the applicability of Fick's second law to chloride ion migration through Portland cement concrete", *Cement Concrete Res.*, **25**(2), 299-303.

- Chen, D. and Mahadevan, S. (2008), "Chloride-induced reinforcement corrosion and concrete cracking simulation", *Cement Concrete Compos.*, **30**(3), 227-238.
- Chen, W.F. (2007), *Plasticity in Reinforced Concrete*, J. Ross Publishing.
- Cheung, M.M., So, K.K. and Zhang, X. (2012), "Life cycle cost management of concrete structures relative to chloride-induced reinforcement corrosion," *Struct. Infrastr. Eng.*, **8**(12), 1136-1150.
- Code, C.E.B.F.I.P.M. (1993), "Design code," *Comite Euro-International du Béton, Bulletin d'Information* **213**(214), 437.
- Fu, C., Jin, X. and Jin, N. (2010), "Modeling of chloride ions diffusion in cracked concrete. Pro-ceedings of the 11th International Conference on Engineering Construction", and Operations in Challenging Environments. United States: American Society of Civil Engineers.
- Fu, C., Jin, X., Ye, H. and Jin, N. (2015), "Theoretical and experimental investigation of loading effects on chloride diffusion in saturated concrete", *J. Adv. Concrete Tech.*, **13**(1), 30-43.
- Guo, Z. (1997), *The Concrete Strength and Deformation: The Basis and the Constitutive Relation*, Tsinghua University Press
- Jeong, J.H. and Zollinger, D.G. (2006), "Finite-element modeling and calibration of temperature prediction of hydrating portland cement concrete pavements", *J. Mater. Civil Eng.*, **18**, 317.
- Lim, C., Gowripalan, N. and Sirivivatnanon, V. (2000), "Microcracking and chloride permeability of concrete under uniaxial compression", *Cement Concrete Compos.*, **22**(5), 353-360.
- Lin, K. and Yang, C. (2014), "A simplified method to determine the chloride migration coefficient of concrete by the electric current in steady state", *Comput. Concr.*, **13**(1), 117-133.
- MacGregor, J. (1988), "Concrete structures: stresses and deformations", *Can. J. Civ. Eng.*, **15**(1), 141-141.
- Papadakis, V.G. (2013). "Service life prediction of a reinforced concrete bridge exposed to chloride induced deterioration", *Adv. Concrete Constr.*, **1**(3), 201-213.
- Paul, S.K., Chaudhuri, S. and Barai, S.V. (2014), "Chloride diffusion study in different types of concrete using finite element method (FEM)", *Adv. Concrete Constr.*, **2**(1), 39-56.
- Saito, M. and Ishimori, H. (1995), "Chloride permeability of concrete under static and repeated compressive loading", *Cement Concrete Res.*, **25**(4), 803-808.
- Van Mien, T., Stitmannathum, B. and Nawa, T. (2009), "Simulation of chloride penetration into concrete structures subjected to both cyclic flexural loads and tidal effects", *Comput. Concr.*, **6**(5): 421-435.
- Van Mien, T., B. Stitmannathum and T. Nawa (2011), "Prediction of chloride diffusion coefficient of concrete under flexural cyclic load", *Comput. Concr.*, **8**(3), 343-355.
- Van Tran, M., B. Stitmannathum and T. Nawa (2009), "Chloride penetration into concrete using various cement types under flexural cyclical load and tidal environment", *IES J. Part A: Civ. Struct. Eng.*, **2**(3), 202-214.
- Yang, C. and Weng, S. (2013), "A multi-phase model for predicting the effective chloride migration coefficient of ITZ in cement-based materials", *Adv. Concrete Constr.*, **1**(3), 239.
- Ye, H., Jin, N., Jin, X. and Fu, C. (2012), "Model of chloride penetration into cracked concrete subject to drying-wetting cycles", *Constr. Build. Mater.*, **36**, 259-269.
- Ye, H., Tian, Y., Jin, N., Jin, X. and Fu, C. (2013), "Influence of cracking on chloride diffusivity and moisture influential depth in concrete subjected to simulated environmental conditions", *Constr. Build. Mater.*, **47**, 66-79.
- Zhang, S., Dong, X. and Jiang, J. (2013), "Effect of measurement method and cracking on chloride transport in concrete", *Comput. Concr.*, **11**(4), 305-316.